GEOPHYSICS, VOL. 57, NO. 12 (DECEMBER 1992); P. 1593–1607, 13 FIGS.

A spectral scheme for wave propagation simulation in 3-D elastic-anisotropic media

José M. Carcione*, Dan Kosloff‡, Alfred Behle**, and Geza Seriani§

ABSTRACT

This work presents a new scheme for wave propagation simulation in three-dimensional (3-D) elastic-anisotropic media. The algorithm is based on the rapid expansion method (REM) as a time integration algorithm, and the Fourier pseudospectral method for computation of the spatial derivatives. The REM expands the evolution operator of the second-order wave equation in terms of Chebychev polynomials, constituting an optimal series expansion with exponential convergence. The modeling allows arbitrary elastic coefficients and density in lateral and vertical directions.

Numerical methods which are based on finite-difference techniques (in time and space) are not efficient when applied to realistic 3-D models, since they require considerable computer memory and time to obtain accurate results. On the other hand, the Fourier method permits a significant reduction of the working space, and the REM algorithm gives machine accuracy with half the computational effort as the usual second-order temporal differencing scheme. The new algorithm provides spectral accuracy for band limited wave propagation with no temporal or spatial dispersion. Hence, the combination REM/Fourier method could be considered at present the fastest and the most accurate of all the algorithms based on spectral methods in terms of efficiency of computer time. The technique is successfully tested with the analytical solution in the symmetry axis of a 3-D homogeneous transversely isotropic solid. Computed radiation patterns in clay shale and sandstone show the characteristics predicted by the theory. A final example computes synthetic seismograms showing the effects of shear-wave splitting of a model where an azimuthally anisotropic cracked shale layer is inside a transversely isotropic sandstone.

INTRODUCTION

The growing importance of 3-D seismic surveys and the predominant 3-D character of anisotropic wavefields requires the development of an efficient and accurate elastic-anisotropic forward modeling code for an appropriate interpretation of the results. For instance, of importance to global seismology is the study of the Earth's crust and upper mantle, which are known to be anisotropic; 3-D polarization analysis in anisotropic media can be used as a structure indicator: in exploration geophysics, particularly in VSP recording, shear-wave splitting has been observed; this phenomenon gives information about the alignment of cracks, an important parameter in reservoir engineering (e.g., Crampin, 1985).

The present approach is based on spectral methods, both in space and time: the Fourier method and the rapid expansion method (REM), respectively. The authors have recently presented a numerical solution algorithm for two-dimensional (2-D) wave modeling in anisotropic media based on the Fourier method and a spectral Chebychev expansion of the evolution operator (Carcione et al., 1988). While the REM method departs from the second-order wave equation, the former uses a first-order differential equation in time. This fact makes the REM twice as fast as the original spectral expansion. On the other hand, the Fourier method

Manuscript received by the Editor August 28, 1991; revised manuscript received May 7, 1992.
*Osservatorio Geofisico Sperimentale, P.O. Box 2011, 34016 Trieste, Italy and Geophysical Institute, Hamburg University, Bundesstrasse 55, 2000 Hamburg 13, Germany.
‡Department of Geophysics and Planetary Sciences, Tel-Aviv University, Tel-Aviv 69978, Israel, and Geophysical Institute, Hamburg University, Bundesstrasse 55, 2000 Hamburg 13, Germany.
**Geophysical Institute, Hamburg University, Bundesstrasse 55, 2000 Hamburg 13, Germany.
§Osservatorio Geofisico Sperimentale, P.O. Box 2011, 34016 Trieste, Italy.

allows using less grid points per wavelength than finite-differencing operators, an essential fact in 3-D wave simulation. Moreover, all the variables are at the same points, avoiding the problem of inaccuracy that the staggered grids cause in anisotropic modeling, where shear strains are at different points than longitudinal strains. Therefore, wavefield computations are highly accurate. Besides this fact, vectorization (mainly the FFT routine) and parallelization of the algorithm provides a very efficient scheme in terms of computer time. The code is optimized to take advantage of the vector and parallel facilities of CRAY systems, particularly the eight processor CRAY Y-MP8E computer using the solid-state storage device (SSD).

The program has been written to compute snapshots and synthetic seismograms in a general anisotropic medium that can be described by 21 independent parameters. The modeling code provides different types of seismic source, directional forces, pressure and shear sources, and the possibility of simulating a free surface. The first section presents the equation of motion of the anisotropic solid. Next, the numerical algorithm is outlined. The modeling is tested against the analytical solution in the symmetry axis caused by a vertical force and a horizontal force. Then, the radiation pattern in a homogeneous clay shale is analyzed. The last example computes synthetic seismograms from a plane-layered structure and a dipping-layered model containing a shale layer with vertical cracks inside a transversely isotropic sandstone.

EQUATION OF MOTION

In a 3-D continuous medium the linearized equations of momentum conservation are

$$\rho \ddot{u}_i = \frac{\partial \sigma_{ij}}{\partial x_j} + \rho f_i, \qquad i = 1, 2, 3, \tag{1}$$

where $\mathbf{x} = (x_1, x_2, x_3) \equiv (x, y, z)$ is the position vector, $\sigma_{ij}(\mathbf{x}, t)$ are the stress components, $u_i(\mathbf{x}, t)$ are the displacements, $\rho(\mathbf{x})$ denotes the density, and $f_i(\mathbf{x}, t)$ are the body forces, t being the time variable. Repeated indices imply summation, and a dot above a variable indicates time differentiation.

The constitutive relation of a 3-D elastic-anisotropic solid is given by

$$\begin{bmatrix} \sigma_{11} \\ \sigma_{22} \\ \sigma_{33} \\ \sigma_{23} \\ \sigma_{13} \\ \sigma_{12} \end{bmatrix} = \begin{bmatrix} c_{11} & c_{12} & c_{13} & c_{14} & c_{15} & c_{16} \\ & c_{22} & c_{23} & c_{24} & c_{25} & c_{26} \\ & & c_{33} & c_{34} & c_{35} & c_{36} \\ & & & c_{44} & c_{45} & c_{46} \\ & & & & c_{55} & c_{56} \\ & & & & & c_{66} \end{bmatrix} \begin{bmatrix} \varepsilon_{11} \\ \varepsilon_{22} \\ \varepsilon_{33} \\ 2\varepsilon_{23} \\ 2\varepsilon_{13} \\ 2\varepsilon_{12} \end{bmatrix}, \tag{2}$$

where

$$\varepsilon_{ij} = \frac{1}{2}\left(\frac{\partial u_i}{\partial x_j} + \frac{\partial u_j}{\partial x_i}\right), \qquad i, j = 1, 2, 3, \tag{3}$$

which are the strain components, and $c_{IJ} = c_{JI}$, $I, J = 1, \ldots, 6$ are the space-dependent elastic coefficients. Equations (1), (2), and (3) can be found in any book dealing with elasticity theory, e.g., Auld (1973).

THE NUMERICAL METHOD

The time integration scheme used to solve the wave equation is the rapid expansion method (REM) (Kosloff et al., 1989). The algorithm requires that the equation of motion be written as

$$\ddot{\mathbf{u}} = -\mathbf{L}^2\mathbf{u} + \mathbf{f}, \tag{4}$$

where $\mathbf{u}$ is the displacement vector, $\mathbf{f}$ is the vector of the body forces, and $-\mathbf{L}^2$ is a linear matrix operator containing the spatial derivatives and the material properties. This matrix operator is expressed by

$$-L_{ij}^2 = \frac{1}{\rho} \nabla_{iJ} c_{JK} \nabla_{Kj}^T, \qquad i, j = 1, 2, 3 \qquad J, K = 1, \ldots, 6, \tag{5}$$

with ∇_{iJ} the components of a spatial derivative operator matrix given by

$$\nabla = \begin{bmatrix} \dfrac{\partial}{\partial x_1} & 0 & 0 & 0 & \dfrac{\partial}{\partial x_3} & \dfrac{\partial}{\partial x_2} \\ 0 & \dfrac{\partial}{\partial x_2} & 0 & \dfrac{\partial}{\partial x_3} & 0 & \dfrac{\partial}{\partial x_1} \\ 0 & 0 & \dfrac{\partial}{\partial x_3} & \dfrac{\partial}{\partial x_2} & \dfrac{\partial}{\partial x_1} & 0 \end{bmatrix}. \tag{6}$$

The formal solution to equation (4) with zero initial conditions is given by

$$\mathbf{u}(\mathbf{x}, t) = \int_0^t \frac{\sin\left[\mathbf{L}(\mathbf{x})(t-\tau)\right]}{\mathbf{L}(\mathbf{x})} \mathbf{f}(\mathbf{x}, \tau)\, d\tau, \tag{7}$$

as can be checked by substitution. Assuming a separable source term of the form

$$\mathbf{f}(\mathbf{x}, t) = \mathbf{g}(\mathbf{x})h(t), \tag{8}$$

the solution (7) can be expressed as

$$\mathbf{u}(\mathbf{x}, t) = \mathbf{G}(\mathbf{x}, t) * h(t), \qquad \mathbf{G}(\mathbf{x}, t) = \frac{\sin\left[\mathbf{L}(\mathbf{x})t\right]}{\mathbf{L}(\mathbf{x})} g(\mathbf{x}), \tag{9}$$

where the symbol "*" denotes time convolution. Note that when $g(\mathbf{x}) = \delta(\mathbf{x})$, the impulse response, $\mathbf{G}(\mathbf{x}, t)$ represents the Green's function of the system.

The REM algorithm is derived by expanding (7) in terms of modified Chebychev polynomials Q_k as follows:

$$\mathbf{u}(t) = \frac{2}{R} \sum_{k=0}^{\infty} b_{2k+1}(t) \frac{R}{i\mathbf{L}} Q_{2k+1}\left(i\frac{\mathbf{L}}{R}\right)\mathbf{g}, \tag{10}$$

where the Q_k's satisfy the following recursion relation

$$Q_{k+2}(s) = (4s^2 + 2)Q_k(s) - Q_{k-2}(s), \qquad Q_1(s) = 1, \qquad Q_3(s) = 4s^3 + 3s, \tag{11}$$

and

$$b_k(t) = \int_0^t J_k(\tau R) h(t - \tau)\, d\tau, \qquad (12)$$

with J_k the kth order Bessel function. R is a positive real number greater than the range of the eigenvalues of the operator $-\mathbf{L}^2$. For 3-D wave propagation, R is taken as $\pi C_{\max}\sqrt{3}/D$, with $C_{\max}$ the highest velocity in the grid and D the minimum grid spacing. Exponential convergence is obtained for a number of terms in equations (10) greater than tR. Actually, the summation can be safely truncated with a k value slightly greater than tR. More details about the method can be found in Kosloff et al., (1989).

Spatial derivatives are calculated by using the Fourier pseudospectral method based on the mixed-radix Fast Fourier transforms (Temperton, 1983), and prime factor Fast Fourier transforms (Temperton, 1988). In this case the length of each FFT is the product of odd prime numbers. Calculations with Nyquist wavenumbers are avoided.

Specific details about the computer implementation of the spatial derivative terms on CRAY computer systems can be found in Reshef et al., (1988). As here, they use the Fourier method to calculate the spatial derivatives, but a second-order finite-difference approach to march the solution in time. This results in an unbalanced scheme with infinite spatial accuracy but only second-order temporal accuracy. Instead, the present algorithm uses both spectral methods in time and space, in this way avoiding any type of numerical dispersion and reaching machine accuracy with efficient performance.

Practical applications of 3-D forward modeling require large quantities of CPU memory. Typical problems need tens of megawords of storage, a size which exceeds the central memory of most computer systems. Implementation of the present algorithm needs three times the number of displacement components at each grid point, three additional arrays for temporal storage, plus the arrays for the elastic coefficients and density, i.e., $M = 15$ for the isotropic case, $M = 18$, for the transversely isotropic case, and $M = 34$ for the general anisotropic case. Total memory requirements are given by $MN_XN_YN_Z$ megawords, a quantity that should not exceed the CPU memory to have efficient performance (N denotes number of grid points).

WAVE PROPAGATION IN HOMOGENEOUS MEDIA

Comparison with analytical solution

The first example compares numerical and analytical solutions in the symmetry axis of a 3-D transversely isotropic medium. The material is defined by the following properties:

$$c_{11} = 66.6 \text{ GPa}, \quad c_{12} = 19.7 \text{ GPa}, \quad c_{13} = 39.4 \text{ GPa},$$

$$c_{33} = 39.9 \text{ GPa}, \quad c_{44} = 10.9 \text{ GPa}, \quad \rho = 2590 \text{ Kg/m}^3,$$

which represent Mesaverde clay shale (Thomsen, 1986). Figure 1 shows a section of the wave surfaces through a plane containing the symmetry axis. Three-dimensional wave surfaces have azimuthal symmetry. This medium is class IV according to the classification given by Payton (1983, p. 38) for which a section of the qSV wave surface has four cuspidal triangles, two centered on the vertical axis and two centered on the horizontal axis. Modes qP and qSV are coupled while SH is pure.

Parameters of the numerical mesh are $N_X = N_Y = N_Z = 119$, with $D_X = D_Y = D_Z = 15$ m, the grid size. The symmetry axis coincides with the vertical axis (Z-axis). The motion is initiated by a directional force with a Ricker time history,

$$h(t) = e^{(1/2)f_0^2(t - t_0)^2} \cos \pi f_0 (t - t_0), \qquad (13)$$

where $t_0 = 60$ ms and $f_0 = 50$ Hz, i.e., a central frequency of 25 Hz. The program ran on an Apollo 10000 computer with vector facilities using about 20 hours of CPU time.

The analytical solution in the symmetry axis is given in the Appendix. For a vertical force, only the vertical displacement u_z is different from zero, while for a horizontal force (say in the X direction), only u_x contributes. Figures 2a and 2b represent the responses of the medium to a unit step $H(t)$ for vertical and horizontal forces, respectively, at a distance of 700 m from the source. The 3-D Green's function or response to the impulse $\delta(t)$ can be calculated by time differentiation. The arrival time of the qP wavefield is t_p, and the lacuna of the qSV mode is between times t_s and t_1 [these times are defined in equations (A-7)]. The singularity at t_1 is not present in an isotropic medium since $\bar{z}_1 = 0$ [by evaluation of (A-9)] and from (A-7) $t_1 \to \infty$. As shown in the next section, this singularity contributes a very high amplitude.

Figures 3a and 3b compare normalized numerical and analytical solutions at a distance of 300 m from the source position, respectively, (a) Z-directional force, and (b) X-directional force. Maximum propagating time of the numerical

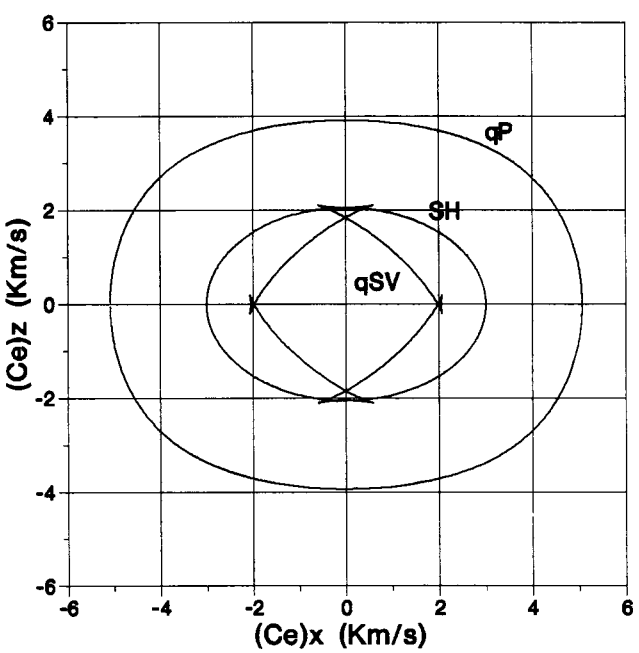

FIG. 1. Zonal section of the energy velocity surfaces in clay shale. The section contains the symmetry axis. Modes qP and qSV are coupled and SH is pure. Cusps can be seen in the qSV wavefront.

seismograms is 0.3 s. As the figures show, the comparison between these solutions is excellent.

Radiation pattern

Snapshots of the wavefield due to an X-directional force are computed for different planes passing through the source position. Figure 4 displays snapshots after $t = 0.22$ s in the XZ, XY, and YZ-planes. The Z-axis is always vertical; in the XY-planes, the Y-axis is vertical. Some characteristics are now discussed. We define the incidence plane by the propagation direction and the Z-axis, qP and qSV motions lie in this plane, while SH motion is normal to the plane. Hence, the u_z component does not contain SH motion.

***XZ*-plane.**—The u_x-component has only qP and qSV motions since SH motion is normal to the plane, although by summetry the u_y component vanishes. The cusps can be distinguished. The higher amplitude is in the symmetry axis where the singularity at time t_1 contributes to the lacuna of the qSV mode. The small contribution of SH motion in the u_x-component could be caused by near source effects.

***XY*-plane.**—Wave surface sections are circles because of isotropy in this plane. The inner wavefront corresponds to the qSV mode. This is a contribution from the slower branches of the qSV mode for which the wavenumber vector is not parallel to the line $Y = 0$. The outer wavefronts are SH and qP motion, respectively. By symmetry, the u_z component vanishes.

***YZ*-plane.**—SH motion is normal to this plane. The characteristic ellipse can be seen in the u_x component. There is a strong contribution from the qSV mode around the line $Y = 0$, due to the singularity in the symmetry axis at time t_1 (see Figures 2a and 2b). As mentioned in the previous section, this contribution is not present in an isotropic medium. By symmetry, the u_y and u_z components have zero amplitude.

It is also verified that snapshots in off-source planes contain the three wave motions except the SH in the u_z-component, as mentioned before.

WAVE PROPAGATION IN INHOMOGENEOUS MEDIA

This example shows wave propagation through a plane-layered structure. A cracked shale layer is enclosed in a transversely isotropic sandstone (vertical symmetry axis). The upper picture in Figure 5 represents a vertical section of the model, and the lower picture is a horizontal section through the shale. This medium is transversely isotropic with symmetry axis horizontal, making an angle of 45 degrees relative to the coordinate axes and horizontal recording lines. The material represents an azimuthally anisotropic solid with vertical cracks.

The media are taken from the table published by Thomsen (1986). They correspond to Taylor sandstone where

$$c_{11} = 34.6 \text{ GPa}, \quad c_{13} = 10.6 \text{ GPa}, \quad c_{33} = 28.3 \text{ GPa},$$

$$c_{55} = 8.4 \text{ GPa}, \quad c_{66} = 12.6 \text{ GPa}, \quad \rho = 2500 \text{ Kg/m}^3,$$

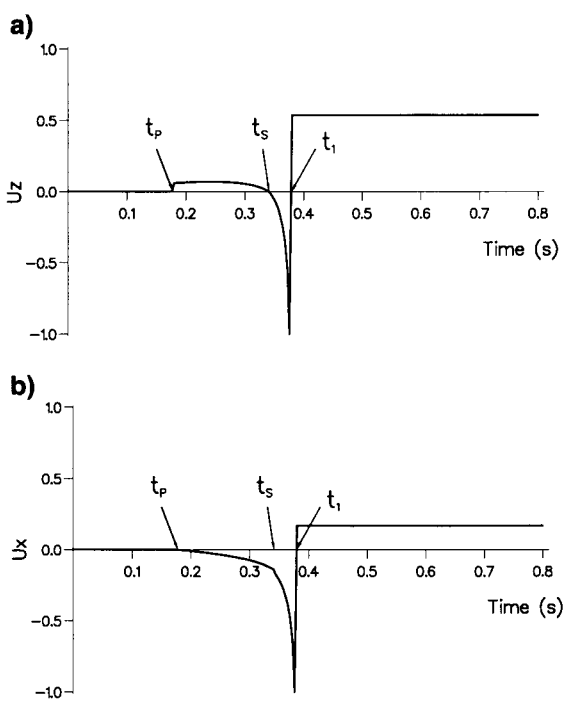

FIG. 2. Analytical displacements for a unit step $H(t)$ time loading function in the symmetry axis of a 3-D transversely isotropic clay shale. (a) Normalized vertical displacement response to a vertical force, and (b) normalized horizontal displacement response to a horizontal force. The distance from the source is 700 m.

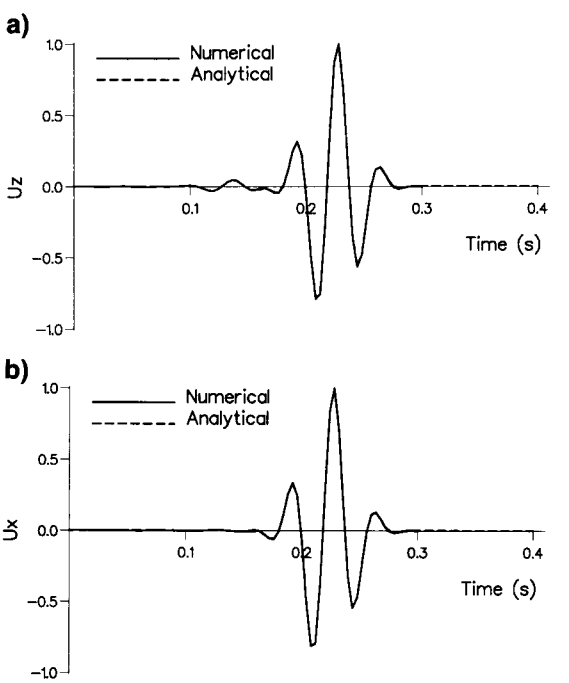

FIG. 3. Comparison between numerical and analytical solutions in the symmetry axis of a 3-D transversely isotropic clay shale. (a) Normalized vertical displacement due to a vertical force, and (b) normalized horizontal displacement due to a horizontal force. The source time function is given by equation (13). The seismograms are recorded at 300 m from the source.

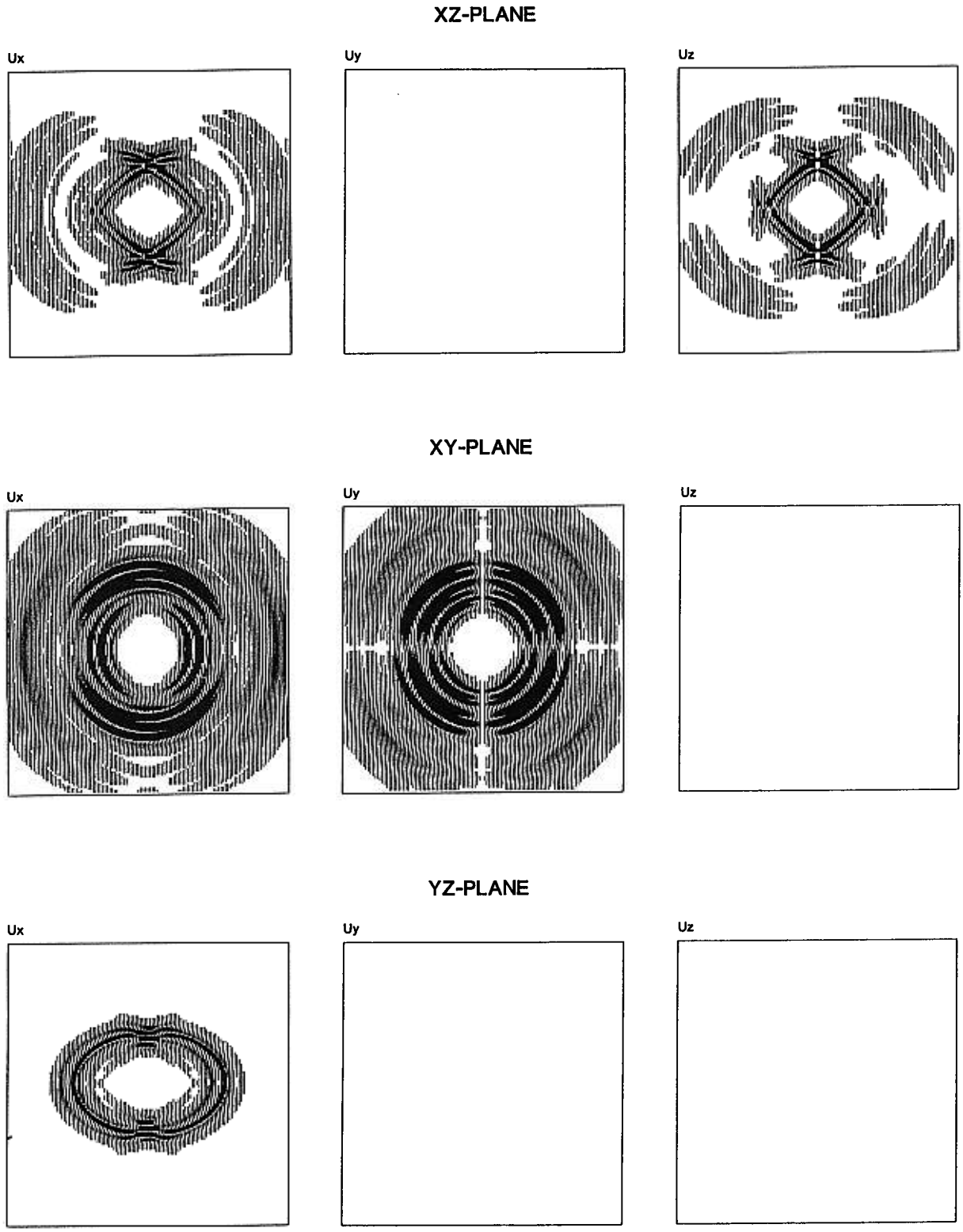

FIG. 4. Radiation pattern in clay shale after $t = 0.22$ s in XY, XZ, and YZ planes passing through the source position. The source is an X-directional force with time function given by equation (13).

and Mesaverde shale (medium without cracks) where

c_{11} = 71.8 GPa, c_{13} = 1.2 GPa, c_{33} = 53.4 GPa,

c_{55} = 26.1 GPa, c_{66} = 34.3 GPa, ρ = 2810 Kg/m^3.

The cracks are introduced by using the theory in Schoenberg and Douma (1988). The strike of the cracks is taken perpendicular to the symmetry axis of the shale. Equation (23) in Schoenberg and Douma is used to obtain the equivalent transversely isotropic solid with cracks, and equation (27) is used to obtain the dimensionless compliances E_N and E_T from Thomsen's parameters ε and y. This example uses ε = 0.15, and γ = 0.1. The elastic coefficients of the transversely isotropic cracked solid become

c_{11} = 71.8 GPa, c_{13} = 0.9 GPa, c_{33} = 39.1 GPa,

c_{55} = 20.1 GPa, c_{66} = 34.3 GPa.

Figure 6 represents a section of the 3-D wave surfaces of the sandstone, and Figure 7 displays sections of the wave surfaces of the shale and the cracked shale, respectively, where the symmetry axis is in the vertical direction. These media are class V according to Payton's classification. The qSV wavefront has four cuspidal triangles (very small), none of which cross the coordinate axes.

For illustration, the radiation pattern for an X-directional force in Taylor sandstone is represented in Figure 8 where propagating time is 0.24 s. For this medium, the solution at the symmetry axis has no singularity at time t_1 in contrast with the clay shale (see Figures 2a and 2b). Therefore, the qSV mode does not contribute significantly to the symmetry axis (see, for instance, YZ-plane in Figure 4). Moreover, since there are no cusps in the XY-plane, there is no qSV motion in this plane (compare Figures 4 and 8).

To get the azimuthally anisotropic medium from the transversely isotropic shale, we perform a clockwise rotation by $\pi/2$ about the X-axis followed by counterclockwise rotation by $\pi/4$ about the new Y-axis. The corresponding rotation matrix is given by equation (18) of Thomsen (1988). The elastic coefficients in the new coordinate system are calculated by using the so-called bond transformations

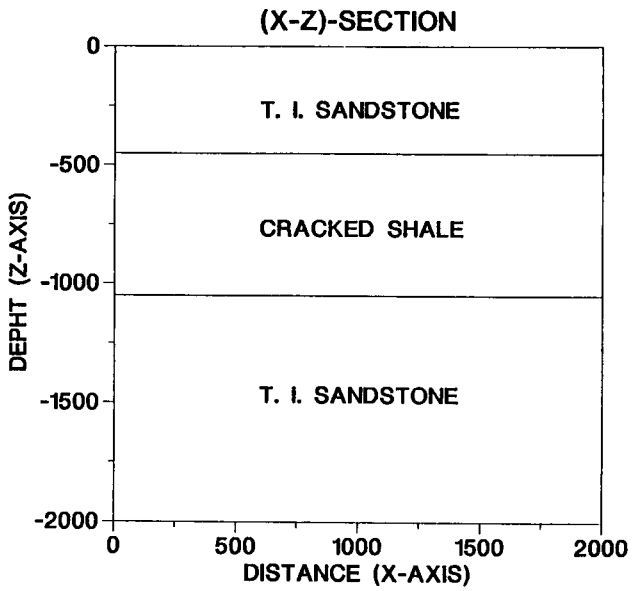

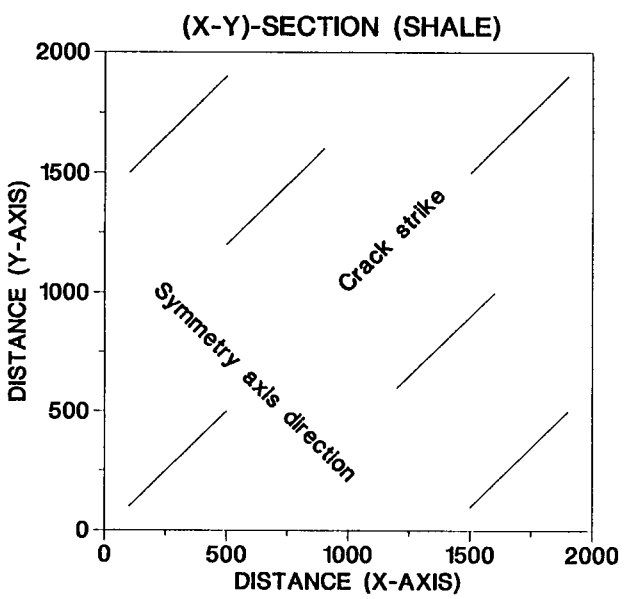

FIG. 5. Plane layered model—vertical and horizontal sections. The sandstone is transversely isotropic with vertical symmetry axis, while the cracked shale is transversely isotropic with horizontal symmetry axis.

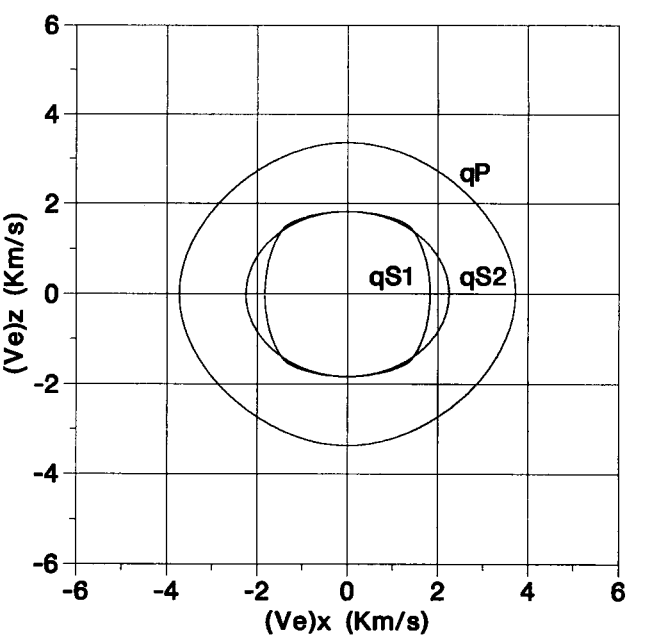

FIG. 6. Zonal section of the energy velocity surfaces in Taylor sandstone. The section contains the symmetry axis.

[equations (3.32) and (3.39) in Auld (1973)]. The nonzero elastic coefficients are

$$c_{11} = 48.2 \text{ GPa}, \quad c_{12} = 8.1 \text{ GPa},$$

$$c_{13} = 2.0 \text{ GPa}, \quad c_{16} = 8.2 \text{ GPa},$$

$$c_{22} = c_{11}, \quad c_{23} = c_{13}, \quad c_{26} = c_{16},$$

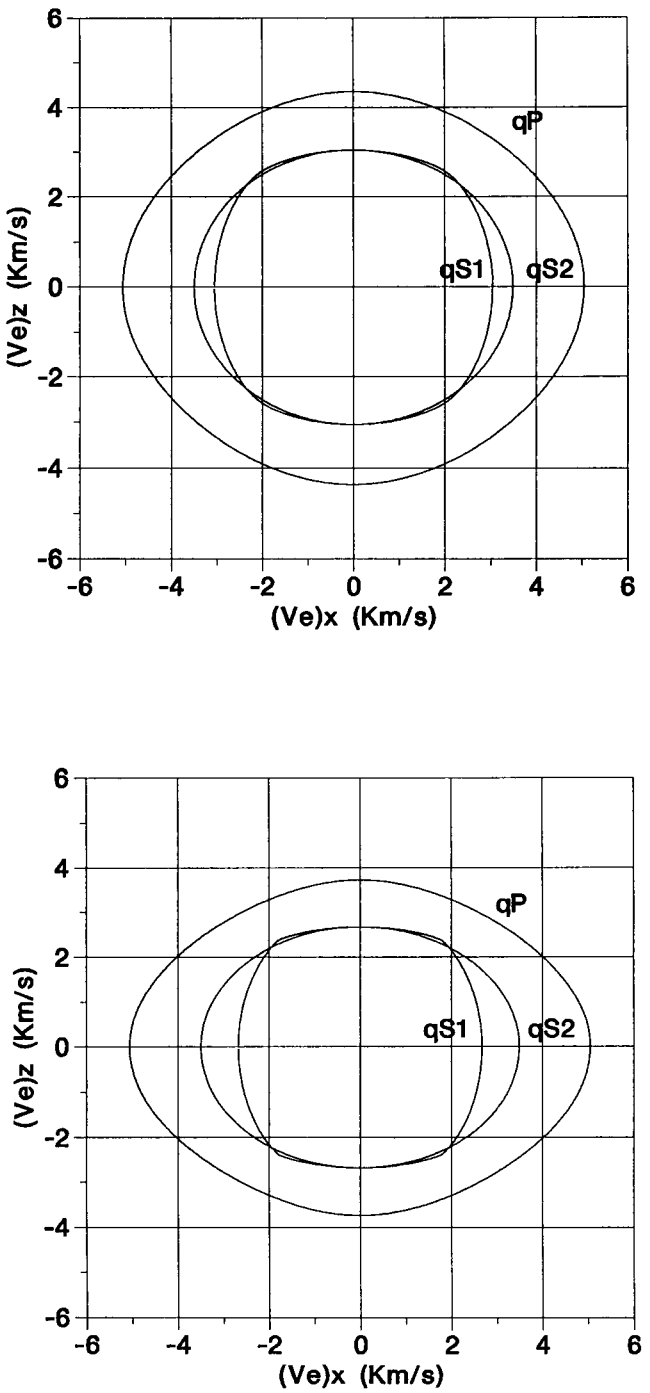

FIG. 7. Zonal section of the energy velocity surfaces in Mesaverde shale (top) and cracked Mesaverde shale (bottom).

$$c_{33} = 71.7 \text{ GPa}, \quad c_{36} = 1.1 \text{ GPa}, \quad c_{44} = 27.2 \text{ GPa},$$

$$c_{45} = 7.1 \text{ GPa}, \quad c_{55} = c_{44}, \quad c_{66} = 27.3 \text{ GPa}.$$

The numerical mesh has a size of $N_X = 135$, and $N_Y = N_Z = 125$ with a grid spacing of $D_X = D_Y = D_Z = 15$ m, including an absorbing region of 18 points on the lateral and bottom edges. No free surface is implemented. The source is a directional force acting in the X-direction with time history given by equation (13) and cutoff frequency of $f_0 = 60$ Hz. The problem requires $34 \times 135 \times 125^2 = 71$ megawords of storage. The program ran on a CRAY Y-MP8E system with 8 CPUs and 128 Mwords of central memory in a wall-clock time of 1.6 hours. Maximum propagating time is 1.5 s.

Figures 9a and 9b represent vertical and horizontal snapshots respectively of the u_x component at a propagating time of 0.5 s. Figure 9a shows two shear waves traveling in the sandstone while in Figure 9b the cracked shale also produces shear-wave splitting but in the vertical direction. Clearly, one shear wave at the top of the shale splits in two at the bottom of the layer. The u_y-component synthetic seismograms of two mutually perpendicular recording lines are represented in Figure 10. $S1$ and $S2$ indicate the two shear events reflected from the bottom of the shale layer. Since the source is X-directional, the P and SH direct events should vanish in the u_y component. This problem comes from the fact that the source is very close to the absorbing region, only two grid points away. What we see are hyperbolas close to straight lines produced by reflection of the direct waves in the absorbing strip. This problem can be solved by taking the source away from this boundary and optimizing the absorbing parameters.

Figure 11 represents the u_x and u_y components in a vertical recording line (VSP). Changes in the slopes of the events are located at the interfaces. From the first interface (450 m depth) the shear waves, one polarized along the cracks ($S1$) and the other perpendicular to the cracks ($S2$) start to separate and are transmitted through the bottom of the shale layer (1050 m depth). Figure 12 shows the u_x and u_y components of the survey line indicated in the upper picture. It can be seen how the reflected events from the bottom of the cracked shale layer arrive at the surface with more traveltime separation. It can be seen how the multiples, although weak, split even more. The last 36 traces are in the absorbing region that appears to have performed very well since the wraparound effect observed in the figures does not reach the model region.

For illustration, a laterally inhomogeneous structure is also considered. This model is composed of the same materials as the previous example but interfaces are dipping as shown in the upper part of Figure 13. The parameters of the numerical mesh are also the same as in the plane layered model. Figure 13 compares u_x components for a vertical recording line. The seismogram of the previous model is at the left, and at the right, the model with dipping layers. Shear-wave splitting is still evident.

CONCLUSIONS

A realistic 3-D seismic survey in exploration geophysics implies at least a 3 km cube region, which by using a 15 m grid spacing gives a 200^3 numerical mesh. For anisotropic wave modeling using the REM algorithm, this means

(text continues on p. 1606)

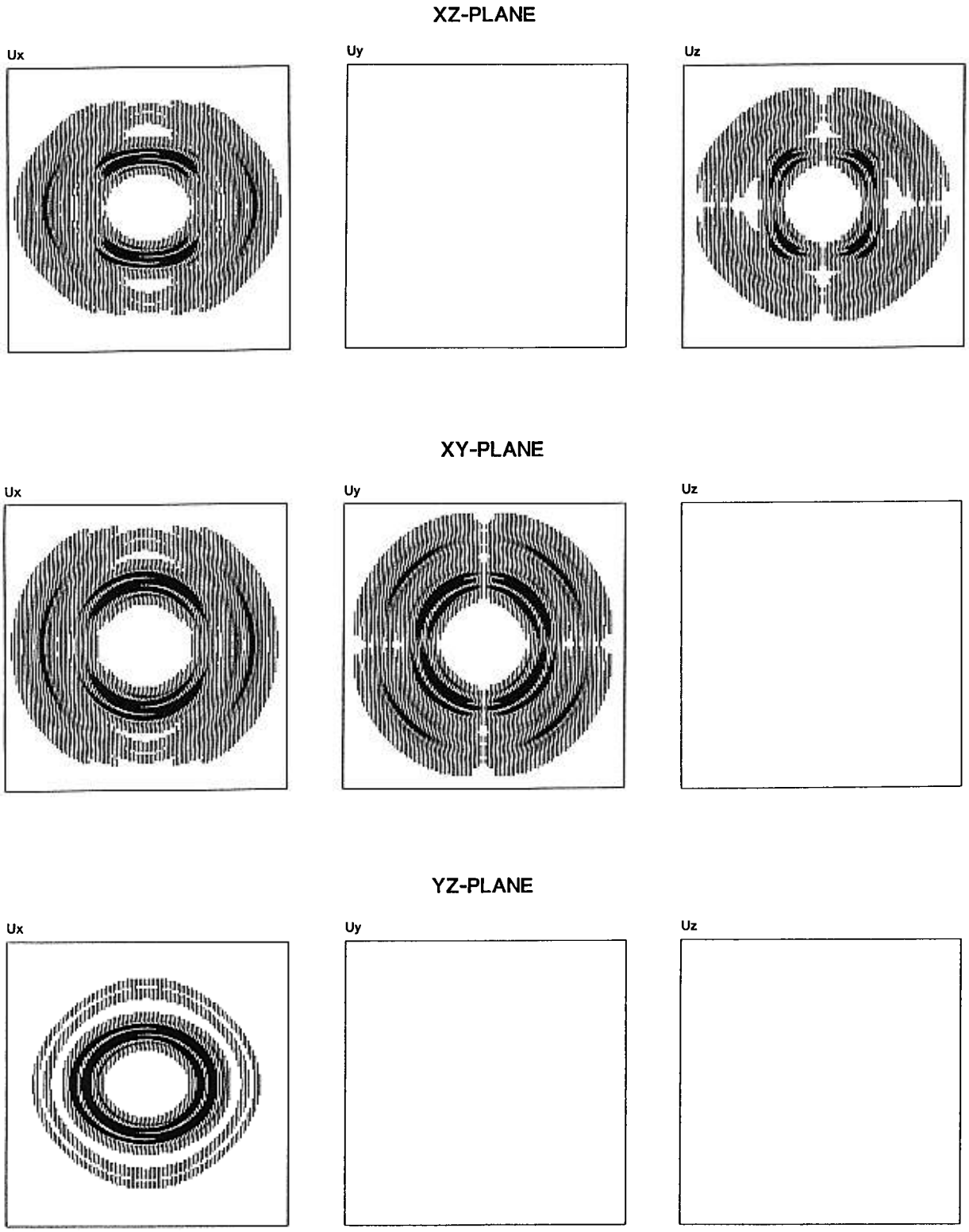

FIG. 8. Radiation pattern in Taylor sandstone due an X-directional force. Propagating time is 0.24 s.

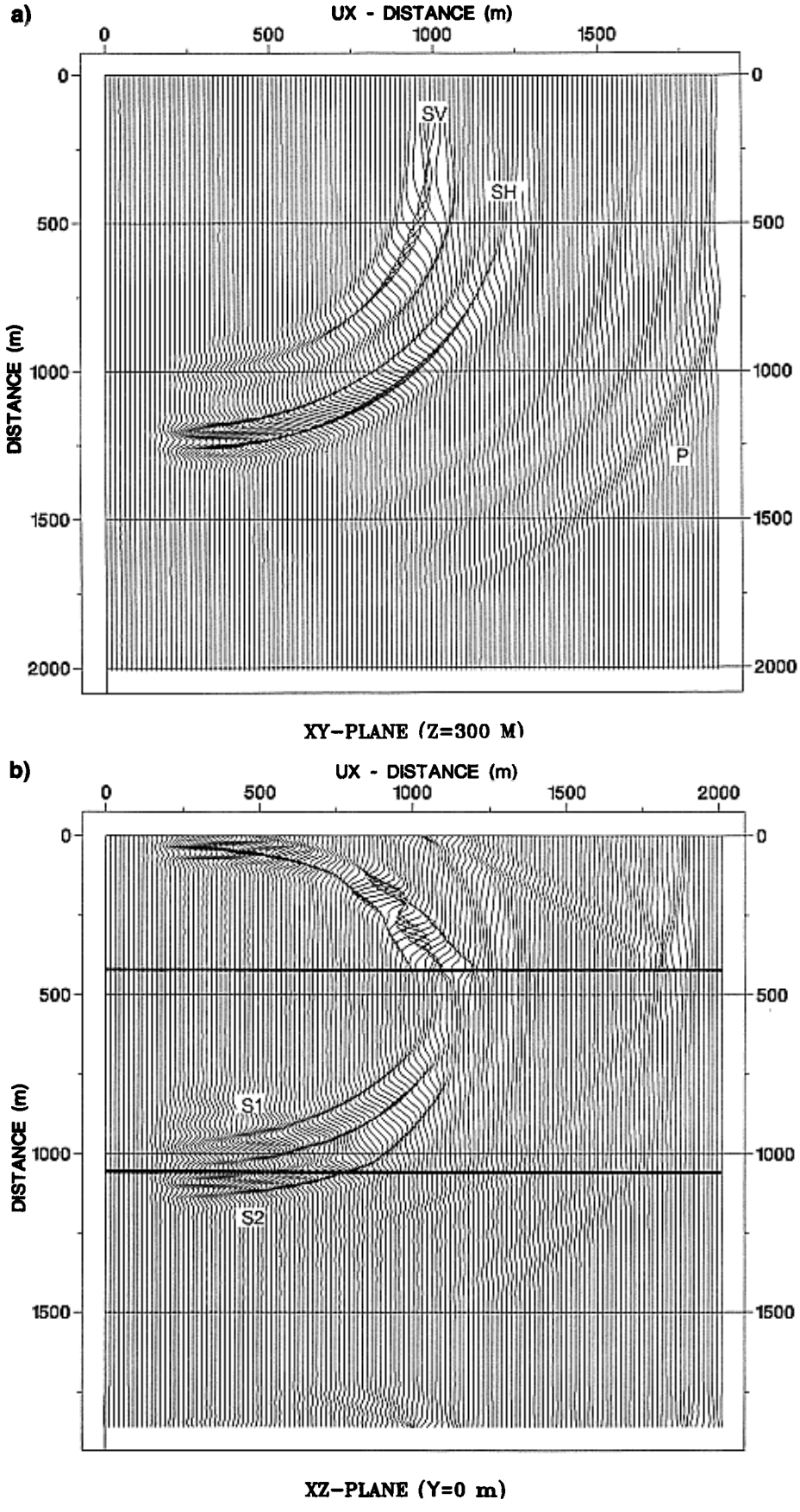

FIG. 9. Snapshots at a propagating time of 0.5 s. (a) The u_x component at 300 m a horizontal plane below the source, and (b) the u_x component in a vertical plane passing through the source location.

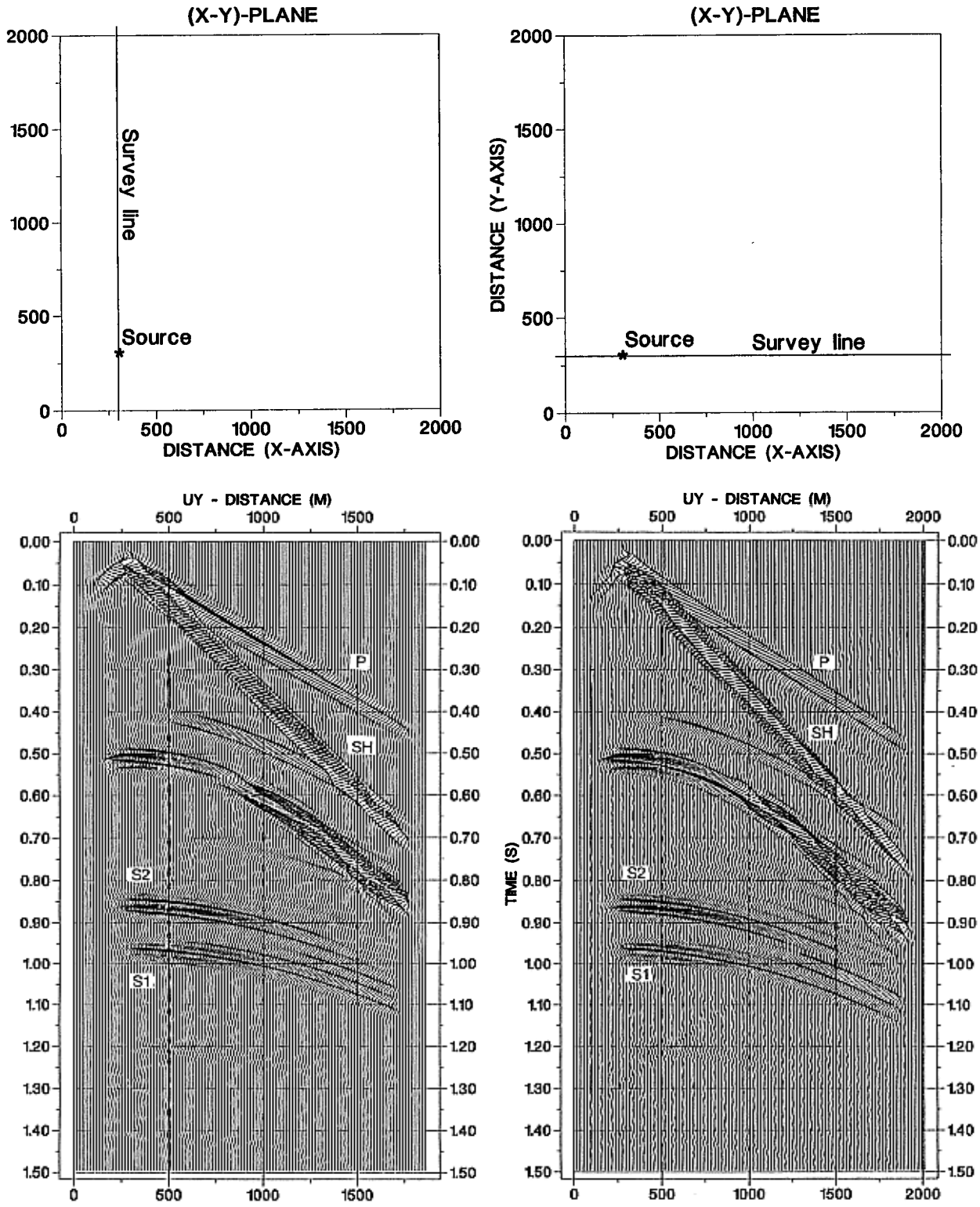

FIG. 10. The u_y component synthetic seismograms of two mutually perpendicular recording lines. $S1$ and $S2$ indicate the two shear events reflected from the bottom of the shale layer.

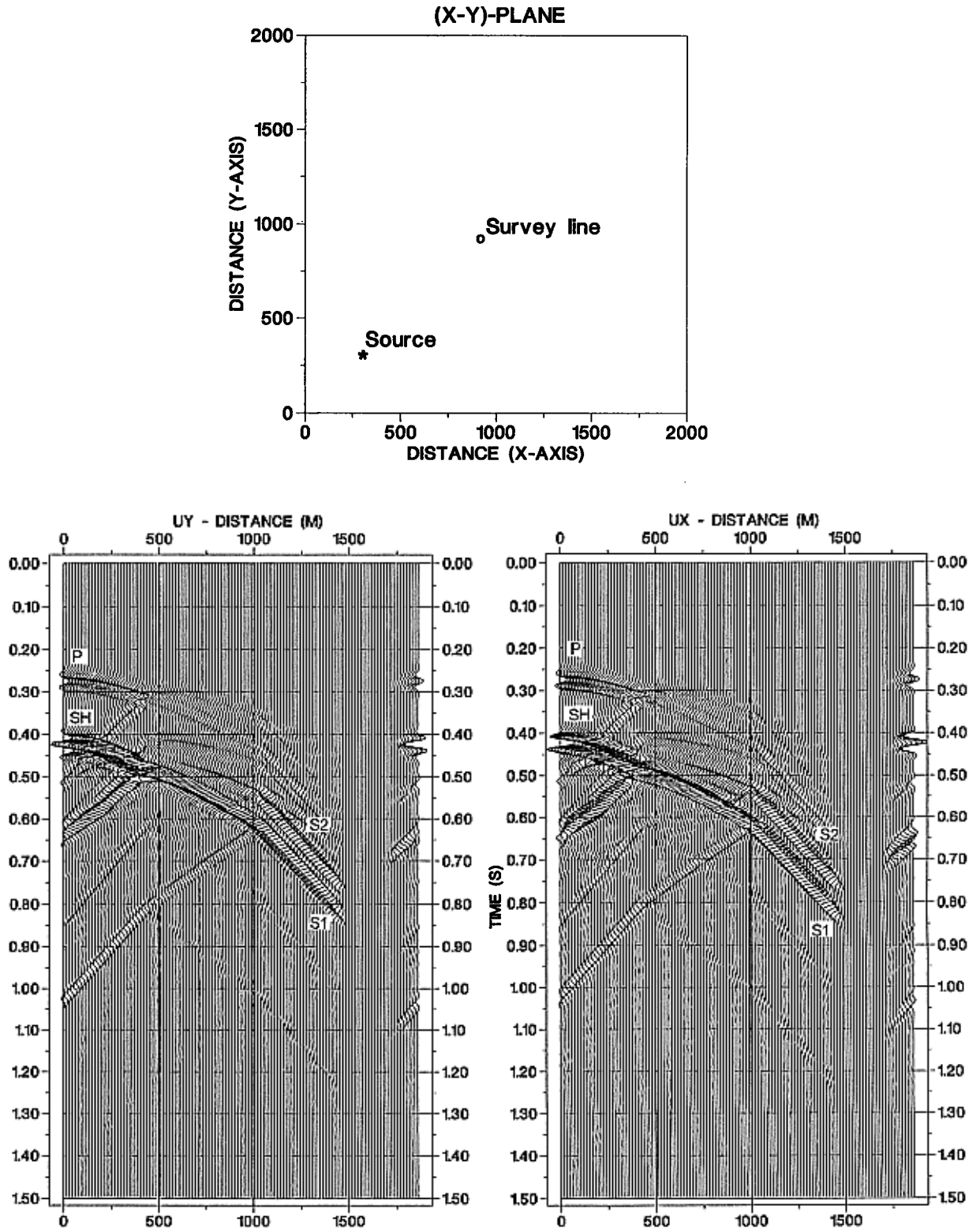

FIG. 11. The u_x and u_y component synthetic seismograms for the recording line are indicated in the upper picture. $S1$ is a shear event polarized along the cracks, while $S2$ has polarization normal to the crack strike.

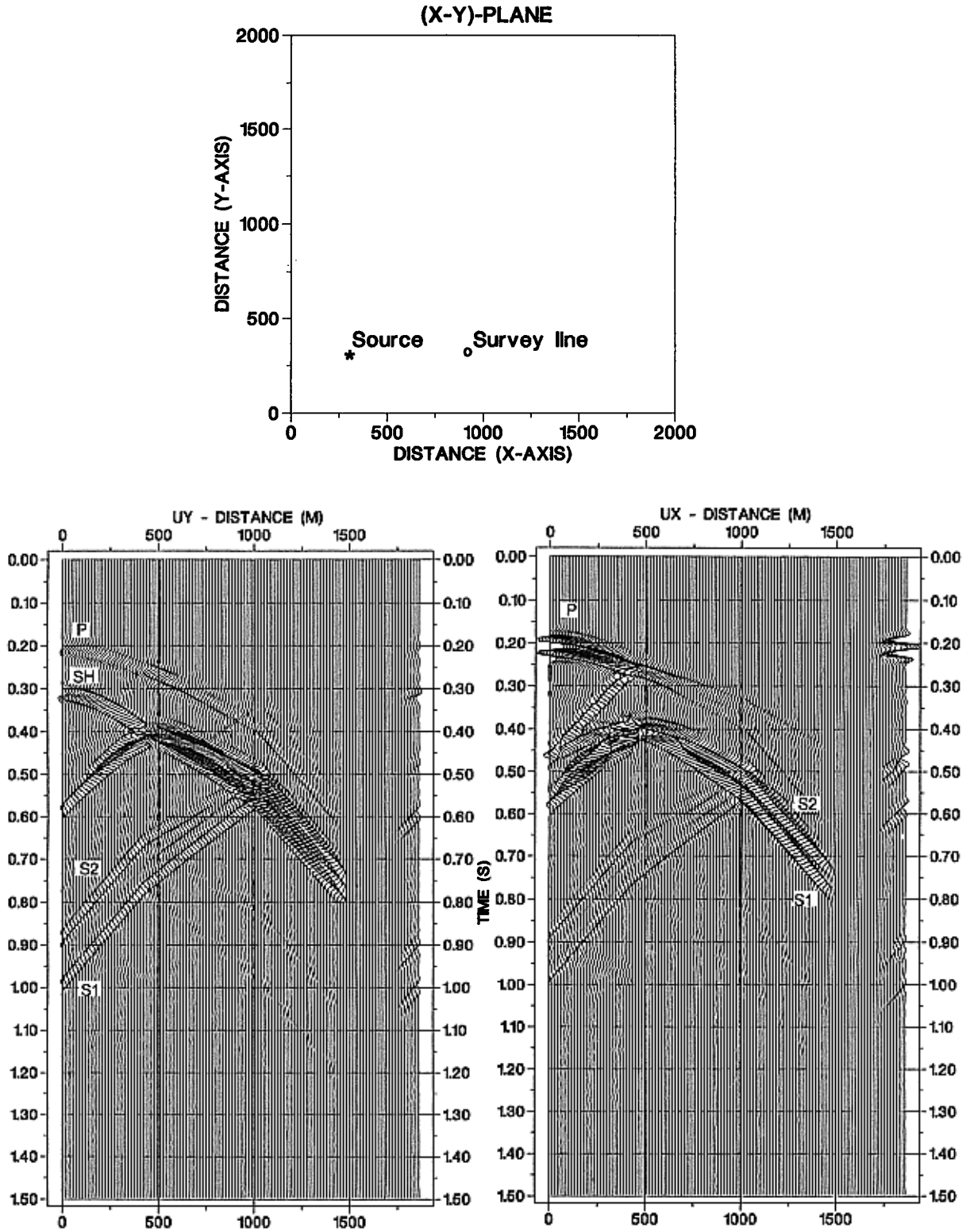

FIG. 12. The u_x and u_y component synthetic seismograms for the recording line are indicated in the upper picture. Shear-wave splitting is greater at the surface. Multiples split even more.

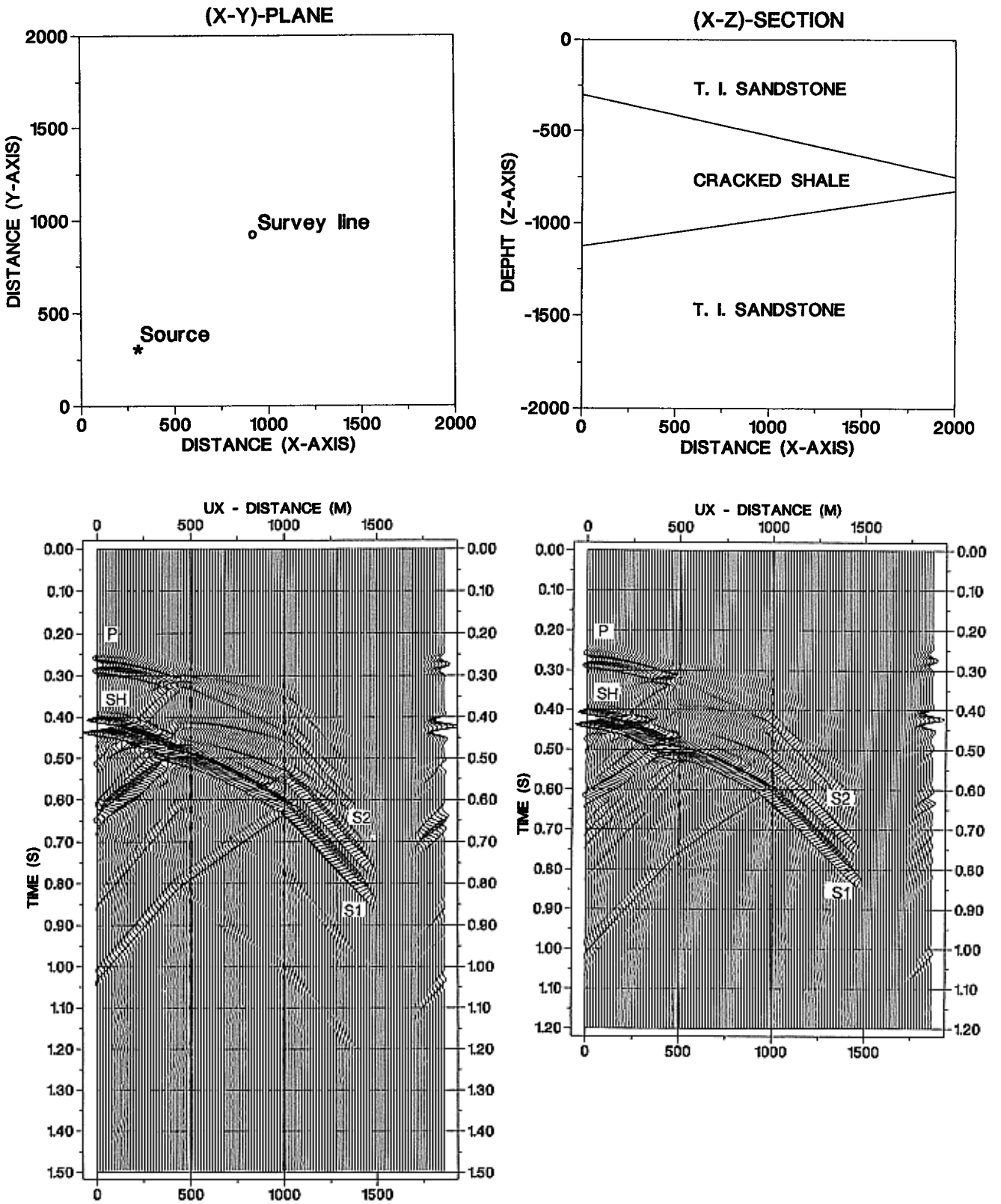

FIG. 13. The u_y component synthetic seismograms for the survey line indicated in the upper picture. At the left, the response of the plane layered model, and at the right, the response of the dipping layered model.

$34 \times 200^3 = 272$ megawords of storage, a feasible problem for today's supercomputers.

The modeling code computes wavefields with spectral accuracy. Errors are associated with spatial discretization of dipping and curved interfaces, and absorbing regions. The first problem requires denser grids, and the second optimization of the absorbing parameters, and moving the source away from the absorbing region since significant artificial reflections occur mainly at grazing angles.

The accuracy of the algorithm is verified in the comparison with analytical solutions in the symmetry axis of a 3-D transversely isotropic solid. Computed wavefronts show the characteristics predicted by the energy velocity surfaces. Amplitude behavior is also predicted by the modeling. For instance, at the point where the *qSV* wavefront crosses itself, there is a contribution that is not present in 3-D isotropic media. A simple structure like the plane layered model shows a characteristic seismic response caused by anisotropy. Rheology proves to be as important as interface geometry. In particular, wave coupling and shear-wave splitting influence the synthetic seismograms. The present modeling technique accurately reproduces these phenomema. A previous computation of the source radiation pattern is useful to interpret the seismograms since each anisotropic solid has its own radiation characteristics, in particular, for the shear modes.

ACKNOWLEDGMENTS

This work was supported in part by the Commission of the European Communities under project GEOSCIENCE. We wish to thank CRAY Research, Inc. for providing computer time.

REFERENCES

Auld, B. A., 1973, Acoustics fields and waves in solids, Vol. 1: John Wiley & Sons, Inc.

Carcione, J. M., Kosloff, D., and Kosloff, R., 1988, Wave propagation simulation in an elastic anisotropic (transversely isotropic) solid: Q. J. Mech. Appl. Math., **41**, 319–415.

Crampin, S., 1985, Evaluation of anisotropy by shear-wave splitting: Geophysics, **50**, 142–152.

Kosloff, D., Queiroz Filho, A., Tessmer, E., and Behle, A., 1989, Numerical solution of the acoustic and elastic wave equations by a new rapid expansion method: Geophys. Prosp., **37**, 383–394.

Payton, R. G., 1983, Elastic wave propagation in transversely isotropic media: Martinus Nijhoff Publ.

Reshef, M., Kosloff, D., Edwards, M., and Hsiung, C., Three-dimensional elastic modeling by the Fourier method: Geophysics, **53**, 1184–1193.

Schoenberg, M., and Douma, J., 1988, Elastic wave propagation in media with parallel fractures and aligned cracks: Geophys. Prosp., **36**, 571–590.

Temperton, C., 1983, Self-sorting mixed-radix fast Fourier transforms: J. Comput. Phys., **52**, 1–23.

——— 1988, Implementation of a prime factor FFT algorithm on CRAY-1: Parallel Comput., **6**, 99–108.

Thomsen, L., 1986, Weak elastic anisotropy: Geophysics, **51**, 1954–1966.

——— 1988, Reflection seismology over azimuthally anisotropic media: Geophysics, **53**, 304–313.

APPENDIX A

ANALYTICAL SOLUTION IN THE SYMMETRY AXIS OF 3-D TRANSVERSELY ISOTROPIC SOLID

The analytical solution is taken from Payton (1983). We define the following dimensionless parameters:

$$\alpha = c_{33}/c_{55}, \qquad \beta = c_{11}/c_{55}, \tag{A-1}$$

$$\gamma = 1 + \alpha\beta - (c_{11}/c_{55} + 1)^2, \qquad \delta = \tfrac{1}{2}(\beta - c_{12}/c_{55}).$$

The solution can be expressed in compact form by using the following dimensionless variable:

$$\bar{z} = \frac{z}{V_S t} \qquad V_S = \sqrt{\frac{c_{55}}{\rho}}, \tag{A-2}$$

where z is the distance to the source along the symmetry axis.

The analytical solution is valid for materials satisfying the inequalities $\gamma < (\beta + 1)$ and $(\gamma^2 - 4\alpha\beta) < 0$.

Vertical force.—The response to

$$\mathbf{f} = (0, 0, 1)\delta(x)\delta(y)\delta(z)H(t), \tag{A-3}$$

where $H(t)$ is the step function, is given by

$$u_x = u_y = 0, \tag{A-4}$$

$$u_z = \frac{1}{4\pi z V_S^2} \begin{cases} 0, & 0 < t \le t_P, \\ h(\bar{z}), & t_P < t \le t_S, \\ 2h(\bar{z}), & t_S \le t < t_1, \\ 1, & t > t_1, \end{cases} \tag{A-5}$$

where

$$h(\bar{z}) = \frac{1}{2} - \frac{2(1 - \bar{z}^2) - \gamma + (\beta + 1)\bar{z}^2}{2\sqrt{D}} \tag{A-6}$$

with

$$t_S = z/V_S, \qquad t_P = z/\sqrt{c_{33}/\rho}, \qquad t_1 = t_S/\bar{z}_1. \tag{A-7}$$

The quantity $D(\bar{z})$ is given by

$$D(\bar{z}) = \{\gamma - (\beta + 1)\bar{z}^2\}^2 - 4\beta(\alpha - \bar{z}^2)(1 - \bar{z}^2) \tag{A-8}$$

and

$$\bar{z}_1 = [\gamma(\beta + 1) - 2\beta(\alpha + 1) + 2\{\beta(1 + \alpha\beta - \gamma)(\alpha + \beta - \gamma)\}^{1/2}]^{1/2}/(\beta - 1). \tag{A-9}$$

Horizontal force.—The response to

$$\mathbf{f} = (1, 0, 0)\delta(x)\delta(y)\delta(z)H(t) \tag{A-10}$$

is given by

$$u_y = u_z = 0, \tag{A-11}$$

$$u_x = \frac{1}{8\pi z V_S^2} \begin{cases} 0, & 0 < t \le t_P, \\ k(\bar{z}), & t_P \le t < t_S, \\ \delta^{-1} + 2k(\bar{z}), & t_S < t < t_1, \\ \delta^{-1} + \beta^{-1}, & t > t_1, \end{cases} \tag{A-12}$$

where

$$k(\bar{z}) = \frac{1}{2\beta} + \frac{(\beta - 1)\bar{z}^2 + (\gamma - 2\alpha\beta)}{2\beta\sqrt{D}}. \tag{A-13}$$

Equations (A-5) and (A-13) are the responses to a unit step $H(t)$. The solution due to a unit impulse $\delta(t)$ is obtained by convolving these expressions with the time derivative of the source time history, equation (13).